Research Article

Advancing PCM Thermal Energy Storage: The Impact of Heat Exchanger Design and Operating Conditions

Mojtaba Semnani Nejad [a], Ahad Khaghani [b], Yasser Rostamiyan [a], Morteza Asghari [b,c]*

[a] *Department of Mechanical Engineering, Sari Branch, Islamic Azad University, Sari, Iran*

[b] *Separation Processes Research Group (SPRG), Department of Chemical Engineering, University of Science and Technology of Mazandaran, Iran*

[c] *UNESCO Chair on Coastal Geo-Hazard Analysis, Tehran-Iran*

ARTICLE INFO

ABSTRACT

This study explores the melting behavior of phase change materials (PCMs) within a triple-tube heat exchanger (TTHX), focusing on the effects of fin geometry, heat exchanger material, and heat transfer fluid (HTF) temperature. A numerical investigation using the enthalpy-porosity technique was performed to evaluate the thermal performance of the system. Results indicate that increasing the number of fins significantly reduces the melting time by enhancing the heat transfer surface area. Among various materials that were tested, copper exhibited the highest thermal conductivity, achieving the fastest melting time and most uniform temperature distribution. Furthermore, raising the heat transfer fluid temperature from 86°C to 98°C reduced the melting time by over 60%, emphasizing the critical role of fluid temperature in the phase change process. These findings provide insights into the design and optimization of phase change material (PCM)-based thermal energy storage systems for applications in building energy management and renewable energy systems.

* Corresponding author.
E-mail address: asghari@mazust.ac.ir; asgharimore@gmail.com

Cite this article as:

1. Introduction

Thermal energy storage systems (TESS) have become essential for optimizing energy management and harnessing environmental energy potential. Phase change materials (PCMs) are now technically mature for building applications and innovations [1-5]. In tubular heat storage units, a PCM can be stored within the tubes while the heat transfer fluid (HTF) flows through the shell, or vice versa. Accordingly, the analyses in the literature reflect the specific configurations used. For instance, Zhang and Faghri [6] analyze a unit where forced laminar convection of water is used as the heat-transfer fluid inside the tube, while the PCM melts in a surrounding hollow cylinder. A similar configuration was studied by Lacroix [7]. Trp et al. [8, 9] investigated the effect of various operating conditions and geometric parameters on a PCM-water shell-and-tube unit. Numerous studies report heat transfer enhancement using axial or radial fins [10-14]. Multi-tube heat transfer arrays have also been explored by Agyenim et al. [15]. More complex configurations include a triplex concentric tube, where the PCM fills the middle channel, a hot HTF flows in the outer channel, and a cold HTF flows in the inner channel [16]. Another configuration features a double pipe with the PCM embedded in a graphite matrix [17].

The use of fins embedded in the PCM is considered the most efficient method for enhancing heat transfer in PCM thermal storage and has been extensively investigated by researchers. This method is appreciated for its simplicity, efficiency, and ease of fabrication [18]. Shatikian et al. [19] presented a numerical study of the melting process of PCM with internal fins exposed to air from the top for electronic cooling purposes. They investigated different fin dimensions, maintaining a constant ratio between fin size and PCM thickness. Wang and Yang [20] numerically studied the cooling technology of portable handheld electronic devices using PCM. They developed a 3D simulation model to investigate the effects of varying fin amounts and heating levels. Labat et al. [21] experimentally investigated a PCM-to-air heat exchanger storage system for building ventilation applications. They studied a prototype heat exchanger containing PCM, designed to provide 1 kW of heating power for 2 hours (i.e., an energy storage of 2 kWh). The exchanger was tested in a closed-loop wind tunnel, which provided constant airflow rates with selected temperature changes to allow the PCM to melt and solidify. Temperature and air velocity measurements were taken at eight airflow rates, and the heating power was estimated. Mosaffa et al. [22] presented an approximate analytical solution for a two-dimensional solidification process of PCM in a shell-and-tube heat exchanger enhanced with radial fins. The variation of the PCM solid fraction with time was compared for cylindrical shells and rectangular storage arrangements with the same volume and heat transfer surface

area. The results indicated that the PCM solidifies more quickly in the cylindrical storage shell than in the rectangular one.

Hosseini et al. [23] investigated the thermal behavior and heat transfer characteristics of Paraffin RT50 as PCM experimentally and numerically during the melting and solidification processes inside a shell-and-tube heat exchanger. The numerical results showed that the melting front appeared at different times at positions closer to the HTF tube, progressing at varying rates outward. Experimental results indicated that by increasing the inlet HTF temperature to 80°C, the theoretical efficiency in the charging and discharging processes rose to 88.4% and 81.4%, respectively. Al-Abidi et al. [24] experimentally investigated the use of a triplex tube heat exchanger with internal-external fins for thermal energy storage. They studied the PCM charging process under steady and unsteady HTF inlet temperatures, as well as the influence of mass flow rates on PCM melting. The PCM solidification process under different mass flow rates was also investigated, and the temperature gradients in the radial and angular directions were analyzed. The results indicated that the HTF inlet temperature had a greater influence on the PCM melting process than the HTF mass flow rate. The charging time was reduced by 58% for HTF mass flow rate and by 86% for HTF inlet temperature.

The use of extended surfaces has shown considerable progress in various heat transfer devices, and utilizing this enhancement could improve the performance of PCM in storage units, which has not been extensively reported in most of the studies mentioned above. In this research, the effect of this enhancement on the thermal characteristics of PCM storage units is considered. The current study investigates the influence of PCM melting from the inside tube, the outside tube, and both tubes. Furthermore, the effects of longitudinal external and internal fins on the melting process in a triplex tube heat exchanger are explored numerically. Finally, the study examines how separating the phase change material with fins, modifying the material heat exchanger, and altering fluid temperatures can improve the performance of PCM-based thermal energy storage.

2. Physical and numerical models

2.1. Physical model

Figure 1 illustrates the physical configuration of the Triple-Tube Heat Exchanger (TTHX). The system consists of an inner tube with a diameter of 50.8 mm and a thickness of 1.2 mm, a middle tube with a diameter of 150 mm and a thickness of 2 mm, and an outer tube with a diameter of 200 mm and a thickness of 2 mm. The tubes are made of stainless steel, nickel, aluminum and

copper while paraffin is used solely as the phase change material (PCM) in the annular space between the inner and middle tubes. The metallic tube walls provide sufficient thermal conductivity to enhance heat transfer between the PCM and both heat transfer fluid (HTF) streams. Different fin numbers and PCM-unit geometries were investigated for Cases A, E, F, and G, as illustrated in Figure 2.
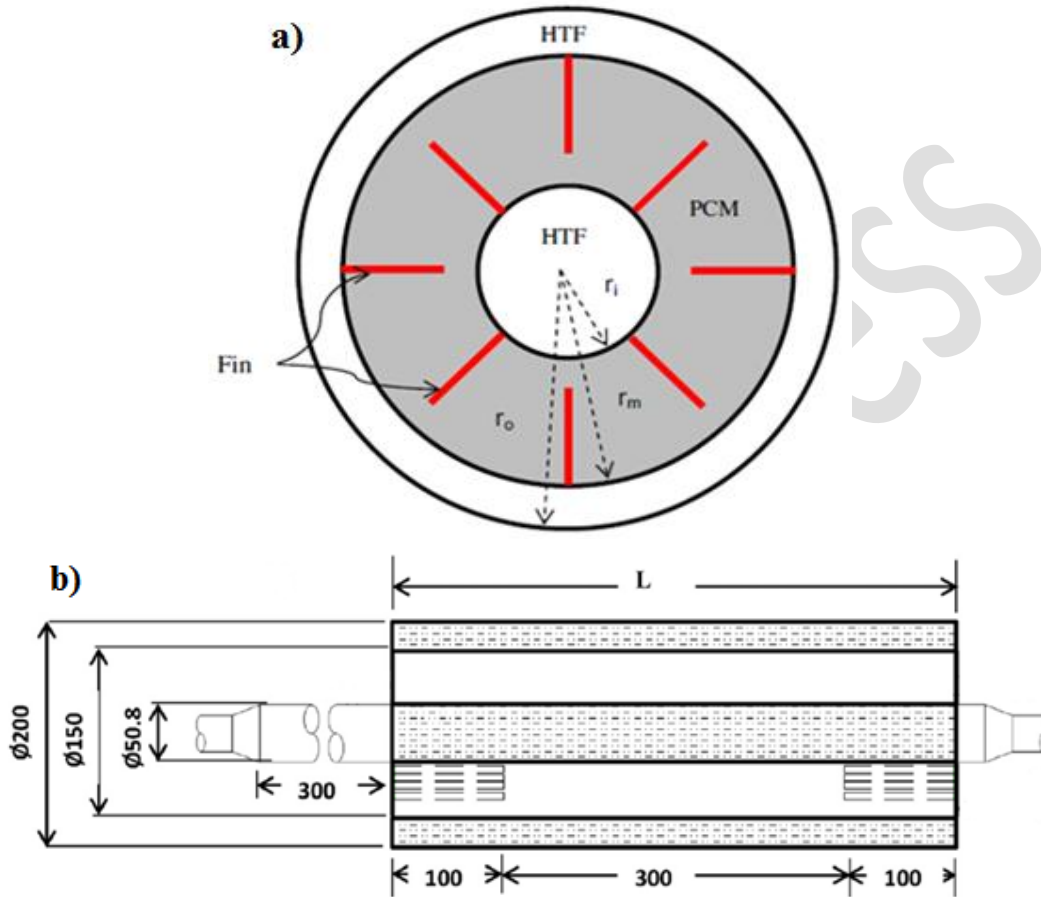

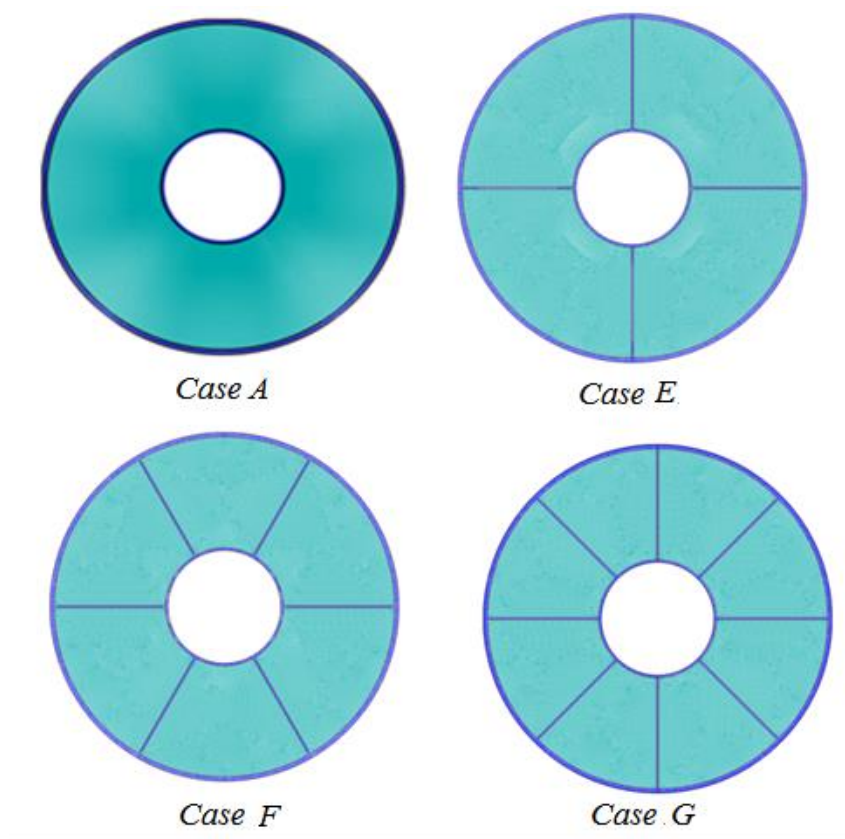**Fig. 1.** (a) Geometry of the studied system, (b) Dimensions of the heat exchanger [24].

Fig. 2. Physical configurations of all investigated cases.

The same fin and tube dimensions were used for both the finned and internally finned tubes, as depicted in Figure 2. The outer and inner tubes are designated for the HTF (water), while the middle tube is used for the PCM, which is based on a commercially available material (paraffin). The thermophysical properties of the materials are provided in Table 1.

Table 1. Thermo-physical properties of the PCM, Paraffin.

Property	Parafina
Density of PCM, solid, $\rho_s \left(\frac{Kg}{m^3}\right)$	950
Specific heat of PCM, liquid, $C_p \left(\frac{J}{Kg.K}\right)$	1868
Latent heat of fusion, $L \left(\frac{J}{Kg}\right)$	176000
Melting temperature, $T_m (C)$	77
Thermal conductivity, $k \left(\frac{W}{m.K}\right)$	0.2
Thermal expansion coefficient $\left(\frac{1}{K}\right)$	0.001
Dynamic Viscosity, $\mu \ (pa.s)$	0.03499

2.2. Governing equation

For the PCM inside the middle tube of the TTHX, the mathematical model of the melting process describes a laminar, unsteady, incompressible flow, with viscous dissipation being

negligible. The analysis assumes constant thermophysical properties for the PCM, including specific heat, thermal conductivity, and viscosity. The effect of natural convection during the melting process is accounted for using the Boussinesq approximation, which is valid for density variations due to buoyancy forces. If the effect of buoyancy is negligible, density variation is disregarded. The density variation is defined as follows:

$$\rho = \frac{\rho_l}{(\beta(T - T_1) + 1)} \qquad \text{(Eq. 1)}$$

where ρ_1 is the density of the PCM at the melting temperature T_l, and β is the thermal expansion coefficient.

Viscous incompressible flow and temperature distribution are solved using the Navier-Stokes and thermal energy equations, respectively. The continuity, momentum, and thermal energy equations are given as follows [25]:

Continuity:

$$\partial_t(\rho) + \partial_i(\rho u_i) = 0 \qquad \text{(Eq. 2)}$$

Momentum:

$$\partial_t(\rho u_i) + \partial_j(\rho u_i u_j) = \mu \partial_{jj} u_i - \partial_i p + \rho g_i + S_i \qquad \text{(Eq. 3)}$$

and the energy equation:

$$\partial_t(\rho h) + \partial_t(\rho \Delta H) + \partial_i(\rho u_i h) = \partial_i(k \partial_i T) \qquad \text{(Eq. 4)}$$

where ρ is the density of the PCM (paraffin), u_i is the fluid velocity, μ is the dynamic viscosity, p is the pressure, g is the acceleration due to gravity, k is the thermal conductivity, and h is the sensible enthalpy. The sensible enthalpy can be expressed as:

$$h = h_{ref} + \int_{T_{ref}}^{T} C_p \Delta T \qquad \text{(Eq. 5)}$$

Enthalpy H can be defined as:

$$H = h + \Delta H \qquad \text{(Eq. 6)}$$

where h_{ref} is the reference enthalpy at the reference temperature T_{ref}, C_p is the specific heat, and ΔH is the latent heat of fusion (PCM), changing between solid and liquid states. The parameter γ represents the liquid fraction during the phase change between solid and liquid, which is the core variable for tracking the phase front in the enthalpy-porosity formulation. This parameter governs the change of state when the temperature T falls within the mushy zone, defined by the solidus temperature T_s and the liquidus temperature T_L ($T_s < T < T_L$). The liquid fraction is defined as [25]:

$$\gamma = \frac{\Delta H}{L} \qquad \text{(Eq. 7)}$$

$$\gamma = \begin{cases} 0 & if\ T < T_s, \\ & , \\ 1 & if\ T > T_l \\ & , \\ \dfrac{T - T_s}{T_l - T_s} & if\ T_s < T < T_l \end{cases} \qquad (Eq.\ 8)$$

The source term S_i in the momentum equation (Eq. 3) is defined as:

$$S_i = \frac{C(1 - \gamma)^2}{\gamma^3} u_i \qquad (Eq.\ 9)$$

Where C is the Mushy zone constant [26], which is a constant reflecting the morphology of the mushy zone, describing how steeply the velocity is reduced to zero as the material solidifies. This constant typically ranges from 10^4 to 10^7 (with 10^5 used for this study) [27].

2.3. Initial and boundary conditions

At the initial time, the PCM was solid, and its temperature was 27°C. The temperature of the heat transfer fluid (HTF) was maintained at a constant value, represented by the tube wall temperature, which was approximately 90°C [28, 29]. The boundary conditions for the TTHX, finned tube, and internally finned tube were varied and can be described as follows:

Heating from both sides method:

$$at\quad r = r_i \rightarrow T = T_{HTF} \qquad (9)$$
$$at\quad r = r_m \rightarrow T = T_{HTF} \qquad (10)$$

Initial temperature for all models:

$$at\quad t = 0 \rightarrow T = T_{ini} \qquad (11)$$

2.4. Numerical modeling

The modeling was performed using FLUENT software, based on the enthalpy-porosity technique and the finite volume method, as outlined by Patankar [30]. In the enthalpy-porosity method, the melt interface is not tracked explicitly. Instead, the liquid fraction, which indicates the fraction of the cell volume that is in liquid form, is computed at each iteration based on enthalpy balance. The mushy zone is a region where the liquid fraction lies between 0 and 1. This zone is treated as a "pseudo-porous medium," where porosity decreases from 1 to 0 as the material solidifies. When the material in a cell has fully solidified, the porosity becomes zero, causing the velocity to drop to zero. For more details on the computational fluid dynamics (CFD) application in latent heat thermal energy storage, refer to [31].

FLUENT 6.3.26, a commercially available program, was used to establish the melting model for simulating the PCM melting process. The two-dimensional geometry (in r and θ) of the TTHX was created and meshed. The mesh generation software Gambit, which is part of the FLUENT software package, was used to define the boundary layers and zone types, and the generated mesh was then exported to FLUENT. The computational grid distribution for the TTHX, including the configuration without fins and the outer and inner wall regions,are presented in figure3. As a further simplification, a half-section computational grid was used to reduce the simulation time. FLUENT uses the finite volume method described in [30] and employs the enthalpy-porosity formulation to solve the mass, velocity, and energy equations.
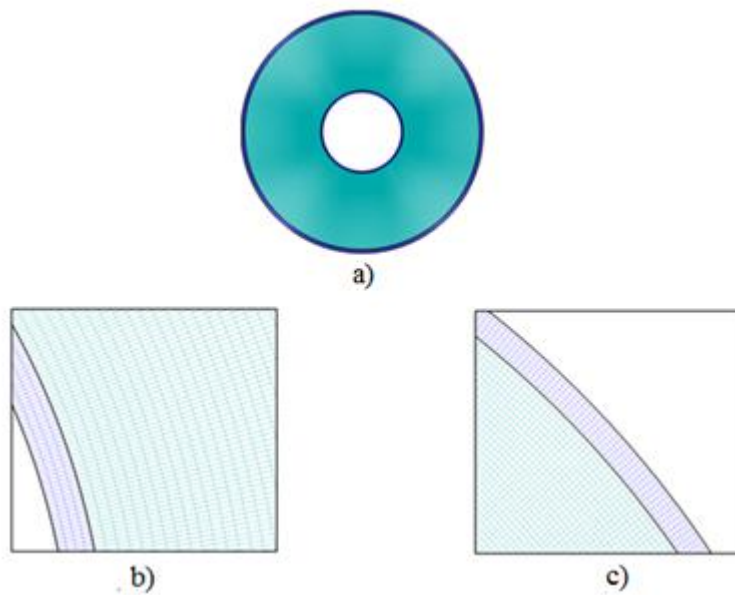

Fig. 3. Computational grid distributions for the TTHX:
(a) Heat exchanger without fins, (b) Outer wall, (c) Inner wall..

For the pressure correction equation, the pressure-staggering option (PRESTO) scheme was used, and the well-known semi-implicit pressure-linked equation (SIMPLE) algorithm was employed for pressure-velocity coupling. The quadratic upwind differencing (QUICK) scheme was used to solve the momentum and energy equations. Figure 4 presents liquid fraction of PCM at the different grid meshing and time steps, which were carefully tested during the initial calculations. The independent time steps and grid sizes for the melt fraction of the TTHX, along with time steps of 0.05 s, 0.25 s (chosen), and 0.5 s, were examined before simulation. In some cases, the time step was initially set to 0.05 s for a few minutes and then increased to achieve quicker convergence, as reported in [32]. Three grid sizes (43,282, 53,850, 64,944 (chosen), and 76,562 cells) were tested to check the grid size independence of the numerical solution. The 64,944-cell grid with a 0.25 s time step was sufficient to achieve the predetermined

convergence for the momentum and energy equations, with convergence criteria of 10^{-5} and 10^{-6}, respectively.

Consider the case of a heat exchanger with fins. To analyze mesh independency solutions, temperature versus time profiles were studied for four different grid configurations, with cell counts of 59,136, 71,868, 87,282, and 105,780 (Fig. 5).

As shown in Figure 5, the temperature-time trace exhibits consistent results, confirming the reliability of the simulation. The third grid, with 87,282 cells, was identified as the optimal configuration with the appropriate fin design. As illustrated in Figure 5, the temperature remains relatively constant over time, with negligible variation, indicating stable results.
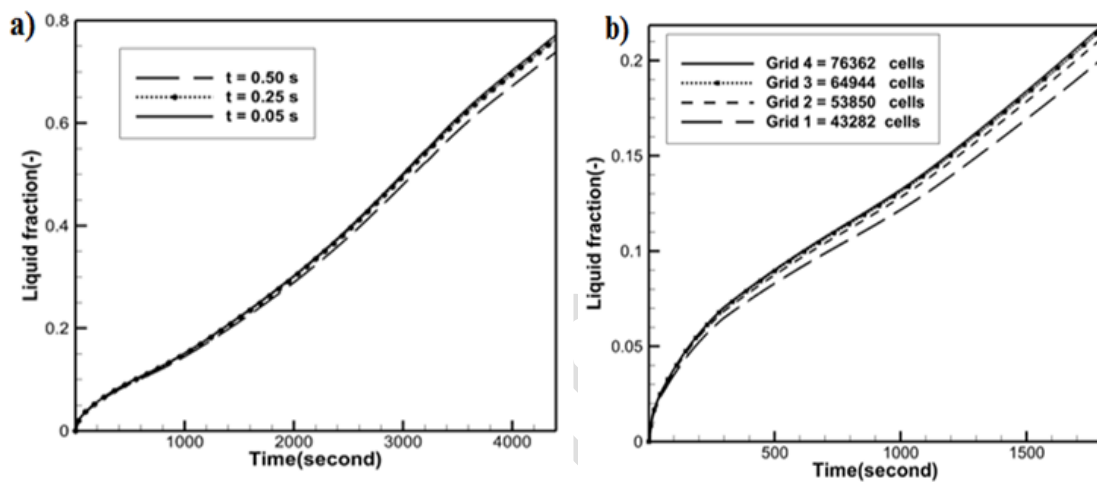

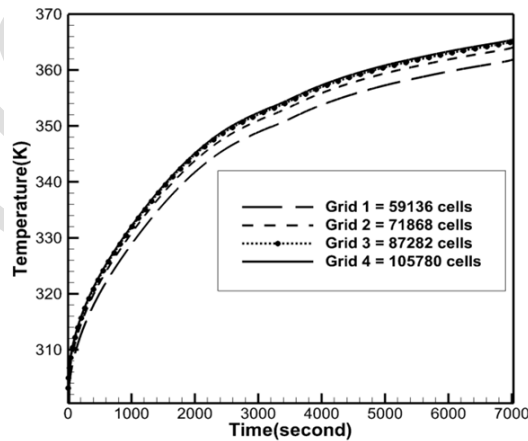**Fig. 4.** Dependence of the numerical solution on (a) time step, and (b) grid size.

Fig. 5. Temperature vs. time for different grid networks..

2.5. Validation of the numerical model

To validate the numerical model, the melting model developed using Fluent 6.3.26 was compared with an experimental setup. This study used the experimental model from Abidi et al. [24] to ensure the accuracy of the numerical model for the PCM melting process. Abidi et

al. fabricated a triplex concentric tube latent heat thermal storage system to validate their numerical model.
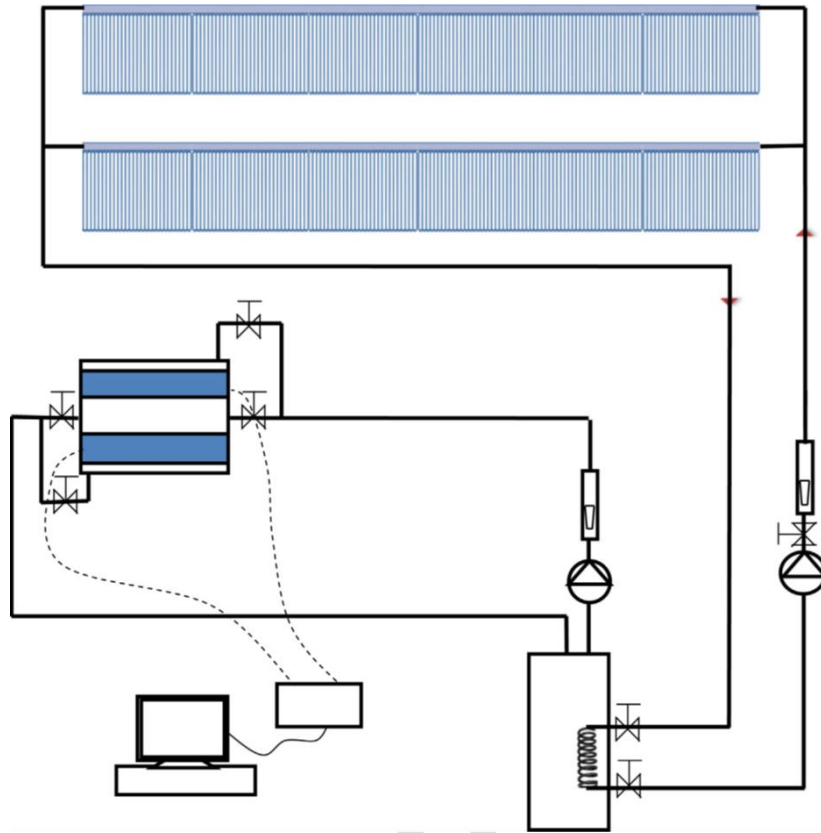

Fig. 6. Schematic diagram of the experimental apparatus, including a triplex concentric tube heat exchanger (TTHX), hot-water circulation pumps (CP), evacuated tube solar collector (ETSC), charging storage tank with an electric heater (CST), rotameter for measuring flow rate (FM), manual shutoff valve (MV), data logger (DL), K-type thermocouples (T-K), and a personal computer (PC) [24].

Figure 6 illustrates a schematic diagram of the experimental apparatus, which includes the TTHX, hot-water circulation pumps, an evacuated tube solar collector (ETSC), a charging storage tank (CST) with an electric heater, a rotameter for measuring flow rate, and a manual shutoff valve. The TTHX section consists of three horizontally mounted concentric tubes, each 500 mm in length, with four longitudinal fins (42 mm fin pitch, 480 mm length, and 1 mm thickness) welded onto both the inner and middle tubes. The geometric parameters of the TTHX are described in the physical model section. The inner tube extends approximately 300 mm from the entrance to ensure fully developed flow.

The data monitoring system includes K-type thermocouples (with 0.5% measurement accuracy), a data logger, and a personal computer to record the temperature distribution in the PCM thermal storage system. The HTF flow rate was measured using a rotameter with a 5% accuracy. A total of 15 thermocouples were installed radially and at different angular directions within the PCM at 10 mm intervals. As shown in Figure 7, the thermocouples were positioned

100 mm from the entrance of the HTF tube in the thermal storage system. To minimize heat loss and insulate the system, 70 mm thick glass wool was wrapped around the TTHX.
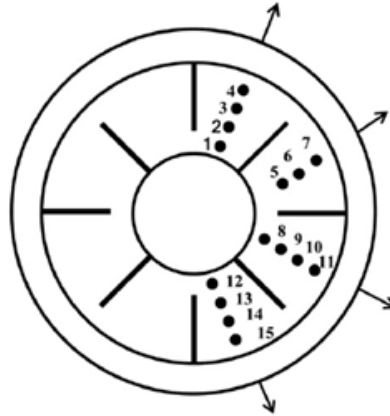

Fig. 7. Schematic diagram and cross-section of the TTHX.

Figure 8 presents the average temperature versus time for the PCM during phase change. The data was collected using the 15 thermocouples, which were strategically placed to monitor temperature changes along the PCM and HTF.

The results from the present numerical model show excellent agreement with the experimental data of Abidi et al. (Figure 7), with a maximum deviation of only 2.8%. Based on these findings, it can be concluded that the current numerical model is valid and accurately represents the PCM melting process.
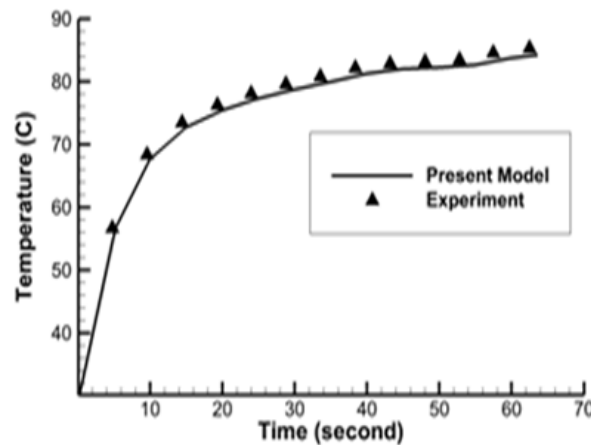

Fig. 8. Comparison of temperature vs. time between the present model and the model by Abidi et al [30].

3. Results and discussion

3.1. Effect of Separating the Phase Change Material with Fins

Figure 9 illustrates the impact of separating the phase change material (PCM) on the melting time using fins. The figure clearly demonstrates that as the PCM is more effectively separated by fins, the melting time decreases. For instance, the complete melting time for Case A (without

fins) is approximately 7060 seconds. Using this case as a baseline (100%), the melting times for other configurations can be calculated. Specifically, the melting times for Cases E, F, and G are reduced to 53.1%, 39.7%, and 36% of the baseline, respectively, summarized in Table 2.

Additionally, Figure 9 indicates that increasing the number of segregated PCM units further reduces the melting time. This improvement is attributed to the increased heat transfer surface area, which enhances heat transfer to the PCM.
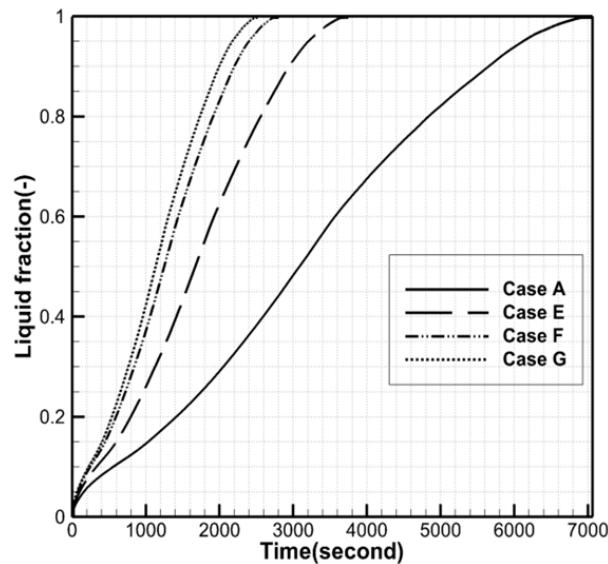

Fig. 9. Liquid fraction of the phase change material with increasing separation of segregated units.

Table 2. The melting time percentage for different number of fin (%)

Case	A	E	F	G
Time(second)	7060	3748.86	2802.82	2541.6
%	100	53.1	39.7	36

Figure 10 depicts the temperature distribution across the segregated PCM units for Cases A, E, F, and G at 1000 seconds from the start of the melting process. The results show that the average temperature increases as the number of segregated units rises, accelerating the melting process.

Figure 11 shows the liquid fraction distribution for Cases A, E, F, and G at 1000 seconds into the melting process. The results highlight that with an increased number of segregated units, a larger portion of the PCM transitions to the liquid phase. Case G demonstrates the most rapid phase change, achieving full liquefaction in the shortest time compared to the other configurations. This result can be attributed to the efficient transfer of heat from the unit's hot surfaces to all the segregated PCM regions in Case G.
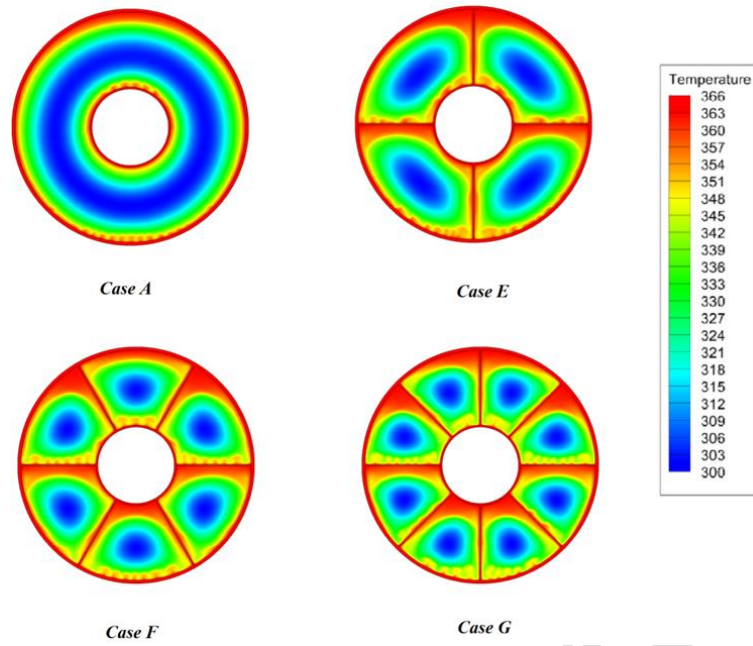
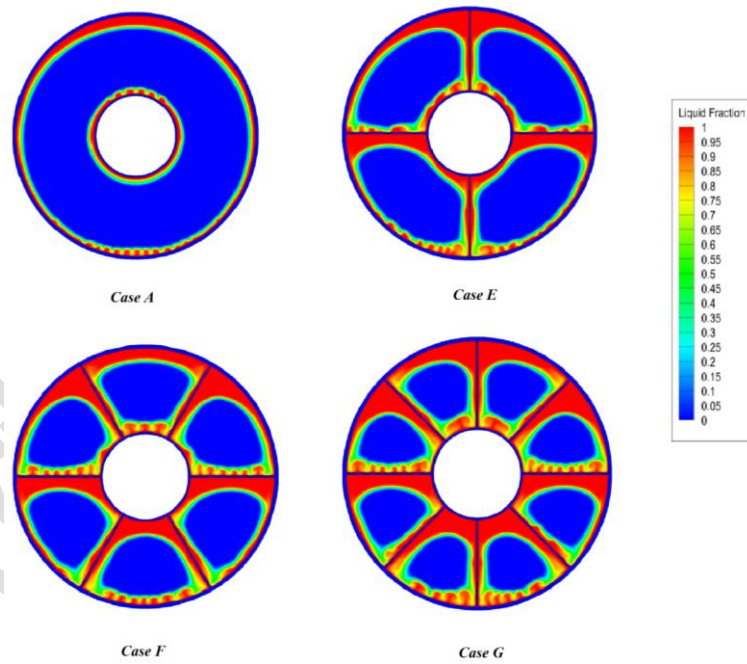**Fig. 10.** Temperature contours at 1000 seconds for the phase change material with increasing segregated units.

Fig. 11. Liquid fraction contours at 1000 seconds for the phase change material with increasing segregated units.

3.2. Effect of Heat Exchanger Material

Figure 12 presents the effect of different heat exchanger materials on the PCM melting time. Among the materials tested (copper, aluminum, nickel, and steel) the PCM in the copper heat exchanger melted the fastest, taking approximately 625.41 seconds. In contrast, the melting times for aluminum, nickel, and steel were 2880, 4260, and 4872 seconds, respectively, as

summarized in Table 3. These differences are due to variations in the thermal conductivity of the materials.

Figure 13 shows the temperature distribution for Case G at 1000 seconds after the onset of the melting process, highlighting the influence of heat exchanger material. The copper heat exchanger demonstrates a more uniform and efficient temperature distribution due to its higher thermal conductivity.
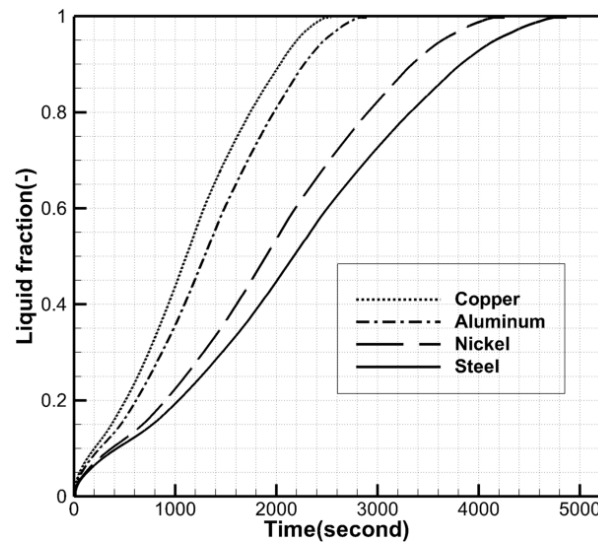

Fig. 12. Liquid fraction vs. time for different heat exchanger materials.

Table 3. Comparison the melting paraffin with a heat exchanger genus change (%).

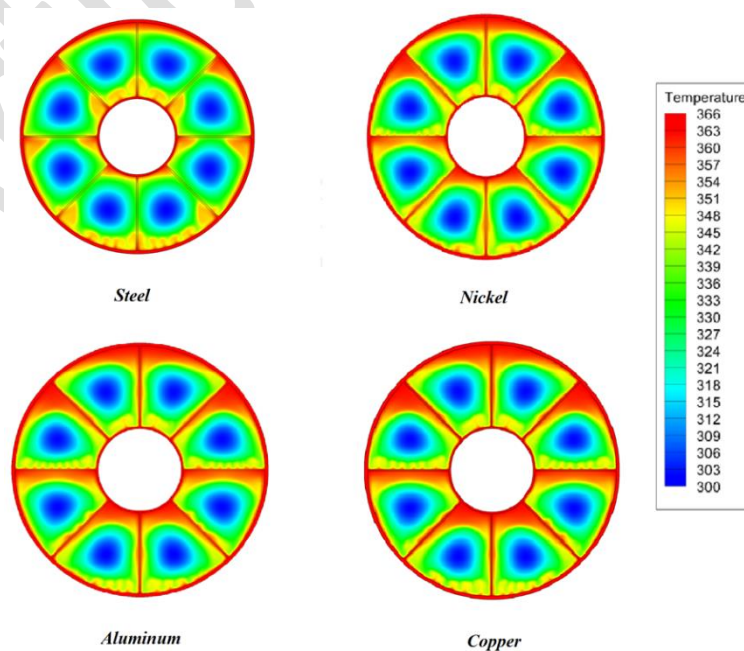| Case G	Steel	Nickel	Aluminum	Copper
Time(second)	4872	4260	2880	2541.6
%	69	60.3	41	36

Fig. 13. Temperature contours at 1000 seconds for different heat exchanger materials.

Figure 14 illustrates the liquid fraction distribution for Case G across the various heat exchanger materials at 1000 seconds from the start of the melting process. The results show that as the thermal conductivity of the material increases (from steel to nickel, aluminum, and copper), a greater portion of the PCM transitions to the liquid phase. This trend highlights the superiority of copper as a heat exchanger material for enhancing the phase change process.
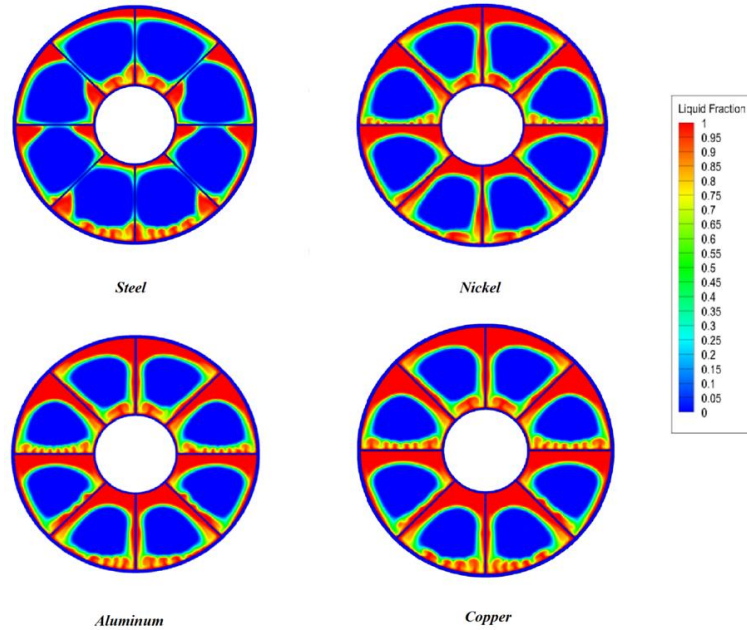

Fig. 14. Liquid fraction contours at 1000 seconds for different heat exchanger materials.

3.3. Effect of fluid temperature

Figure 15 illustrates the effect of fluid temperature on the melting process of the phase change material (PCM). The results indicate that higher fluid temperatures significantly reduce the PCM melting time. Specifically, the PCM melts more quickly with heat exchanger fluid temperatures of 86°C, 90°C, 94°C, and 98°C, respectively. For example, the complete melting time for a fluid temperature of 86°C is approximately 4140 seconds. For fluid temperatures of 90°C, 94°C, and 98°C, the melting times are reduced to 2541 seconds, 1980 seconds, and 1626 seconds, respectively. These results are summarized in Table 4.
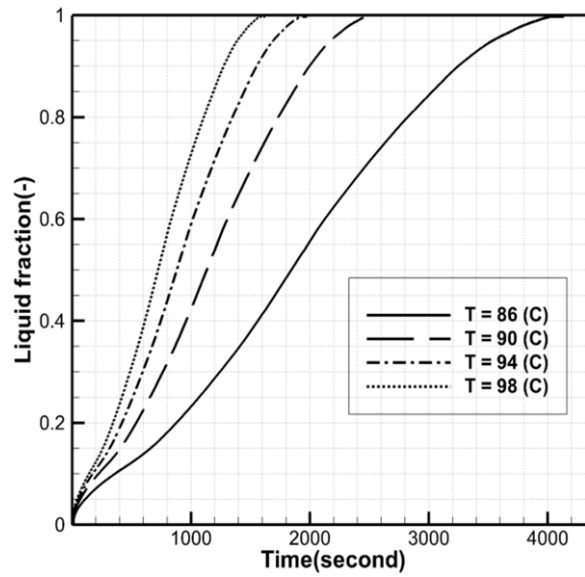
Fig. 15. Liquid fraction vs. time for different fluid temperatures.

Table 4. The melting time percentage for different fin thickness (%).

T_i (°C)	86	90	94	98
Time(second)	4140	2541.6	1980	1626
%	58.6	36	28	23

Figure 16 shows the temperature distribution for Case G as a function of fluid temperature changes after 1000 seconds from the start of the melting process. The results reveal that as the fluid temperature increases (86°C, 90°C, 94°C, and 98°C), the average temperature within the PCM also rises, leading to faster phase transitions.

Figure 17 depicts the liquid fraction distribution during the melting process for Case G under varying fluid temperatures after 1000 seconds. The results demonstrate that higher fluid temperatures result in a greater proportion of the PCM transitioning to the liquid phase. This confirms the significant influence of fluid temperature on accelerating the phase change process and enhancing overall heat transfer efficiency.
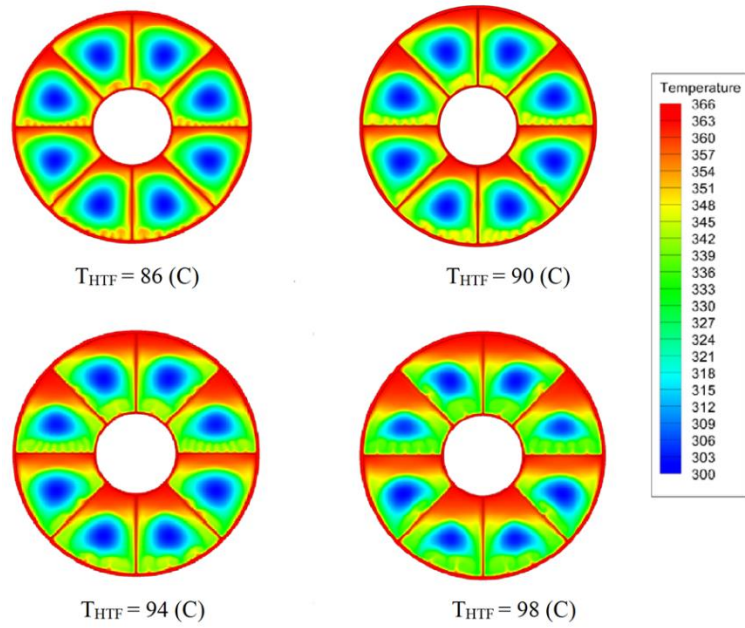
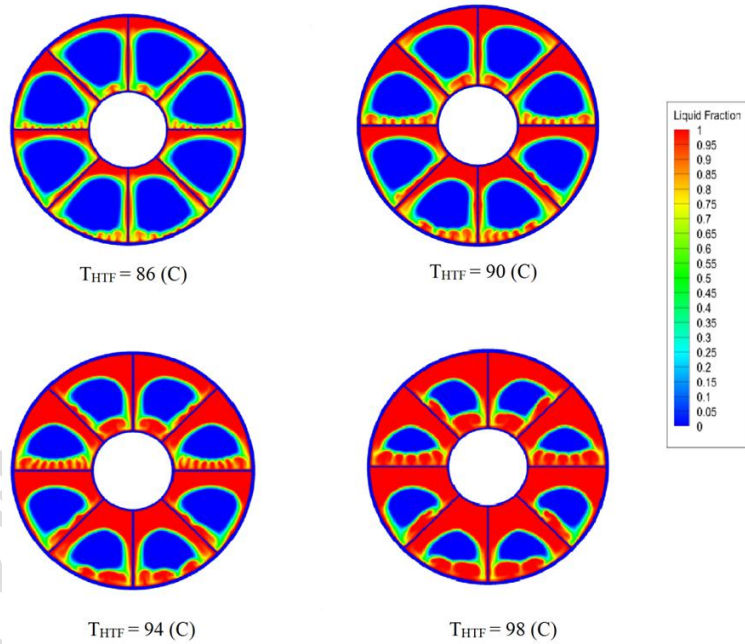**Fig. 16.** Temperature contours at 1000 seconds for different fluid temperatures.

Fig. 17. Liquid fraction contours at 1000 seconds for different fluid temperatures.

4. Conclusion

This study numerically investigated the melting behavior of phase change materials (PCMs) in a triple-tube heat exchanger (TTHX) under various configurations, focusing on the effects of fin geometry, heat exchanger material, and fluid temperature. Key findings include:

1. **Effect of Fins:** Increasing the number of segregated units via fins significantly enhanced heat transfer efficiency and reduced melting time. The configuration with the highest fin density (Case G) demonstrated the shortest melting time, attributed to an increased heat transfer surface area and improved thermal distribution.

2. **Heat Exchanger Material:** The thermal conductivity of the heat exchanger material profoundly influenced the PCM melting process. Copper, with its superior thermal conductivity, outperformed other materials (aluminum, nickel, and steel), achieving the fastest melting time and the most uniform temperature distribution.

3. **Fluid Temperature:** Higher heat transfer fluid (HTF) temperatures markedly reduced the PCM melting time. For fluid temperatures ranging from 86°C to 98°C, the melting time decreased by over 60%, highlighting the critical role of HTF temperature in accelerating the phase change process.

The results underscore the importance of optimizing fin geometry, material selection, and fluid temperature to enhance the thermal performance of PCM-based heat exchangers. These findings provide valuable insights for designing efficient thermal energy storage systems, particularly for applications in building heating, cooling, and renewable energy systems. Future studies could explore the integration of dynamic heat flux and advanced materials to further improve PCM performance.

Conflicts of Interest

The author declares that there is no conflict of interest regarding the publication of this article.

References

[1] A. Waqas, Z.U. Din, Phase change material (PCM) storage for free cooling of buildings: a review, Renewable and Sustainable Energy Reviews 18 (2013) 607–625.

[2] E. Halawa, W. Saman, Thermal performance analysis of a phase change thermal storage unit for space heating, Renewable Energy 36 (1) (2011) 259–264.

[3] V. Dubovsky, G. Ziskind, R. Letan, Analytical model of a PCM-air heat exchanger, Applied Thermal Engineering 31 (16) (2011) 3453–3462.

[4] J. Borderon, J. Virgone, R. Cantin, F. Kuznik, Full-scale study of a building equipped with a multi-layer rack latent heat thermal energy storage system, HVAC&R Research 17 (4) (2011) 566–576.

[5] P. Dolado, J. Mazo, A. Lazaro, J. Maria, B. Zalba, Experimental validation of a theoretical model: uncertainty propagation analysis to a PCM-air thermal energy storage unit, Energy and Buildings 45 (2012) 124–131.

[6] Y. Zhang, A. Faghri, Semi-analytical solution of thermal energy storage system with conjugate laminar forced convection, Int. J. Heat Mass Transfer 39 (1996) 717–724.

[7] M. Lacroix, Numerical simulation of a shell-and-tube latent heat thermal energy storage unit, Sol. Energy 50 (1993) 357–367.

[8] A. Trp, An experimental and numerical investigation of heat transfer during technical grade paraffin melting and solidification in a shell-and-tube latent thermal energy storage unit, Sol. Energy 79 (2005) 648–660.

[9] A. Trp, K. Lenic, B. Frankovic, Analysis of the influence of operating conditions and geometric parameters on heat transfer in water-paraffin shell-and-tube latent thermal energy storage unit, Appl. Thermal Eng. 26 (2006) 1830–1839.

[10] Y. Zhang, A. Faghri, Heat transfer enhancement in latent heat thermal energy storage system by using the internally finned tube, Int. J. Heat Mass Transfer 39 (1996) 3165–3173.

[11] K.A.R. Ismail, C.L.F. Alves, M.S. Modesto, Numerical and experimental study on the solidification of PCM around a vertical axially finned isothermal cylinder, Appl. Thermal Eng. 21 (2001) 53–77.

[12] A. Erek, Z. Ilken, M.A. Acar, Experimental and numerical investigation of thermal energy storage with a finned tube, Int. J. Energy Res. 29 (2005) 283–301.

[13] K. Ermis, A. Erek, I. Dincer, Heat transfer analysis of phase change processes in a finned-tube thermal energy storage system using artificial neural network, Int. J. Heat Mass Transfer 50 (2007) 3163–3175.

[14] F. Agyenim, P. Eames, M. Smyth, A comparison of heat transfer enhancement in a medium temperature thermal energy storage heat exchanger using fins, Sol. Energy 83 (2009) 1509–1520.

[15] F. Agyenim, P. Eames, M. Smyth, Heat transfer enhancement in medium temperature thermal energy storage system using a multitube heat transfer array, Renew. Energy 35 (2010) 198–207.

[16] Long Jian-you, Numerical and experimental investigation for heat transfer in triplex concentric tube with phase change material for thermal energy storage, Sol. Energy 82 (2008) 977–985.

[17] M. Medrano, M.O. Yilmaz, M. Nogues, I. Martorell, J. Roca, L.F. Cabeza, Experimental evaluation of commercial heat exchangers for use as PCM thermal storage systems, Appl. Energy 86 (2009) 2047–2055.

[18] A.A. Al-Abidi, S. Mat, K. Sopian, M.Y. Sulaiman, A.T. Mohammad, Experimental study of PCM melting in triplex tube thermal energy storage for liquid desiccant air conditioning system, Energy and Buildings 60 (2013) 270–279.

[19] V. Shatikian, G. Ziskind, R. Letan, Numerical investigation of a PCM-based heat sink with internal fins, Int. J. Heat Mass Transfer 48 (2005) 3689–3706.

[20] Y.-H. Wang, Y.-T. Yang, Three-dimensional transient cooling simulations of a portable electronic device using PCM in a multi-fin heat sink, Energy 36 (2011) 5214–5224.

[21] M. Labat, J. Virgone, D. David, F. Kuznik, Experimental assessment of a PCM-to-air heat exchanger storage system for building ventilation applications, Appl. Thermal Eng. 71 (2014) 117–123.

[22] A.H. Mosaffa, F. Talati, H.B. Tabrizi, M.A. Rosen, Analytical modeling of PCM solidification in a shell-and-tube finned thermal storage for air conditioning systems, Energy Build. 49 (2012) 356–361.

[23] M.J. Hosseini, M. Rahimi, R. Bahrampouri, Experimental and computational evaluation of a shell-and-tube heat exchanger as a PCM thermal storage system, Int. Commun. Heat Mass Transfer 44 (2013) 32–38.

[24] A.A. Al-Abidi, S. Mat, K. Sopian, M.Y. Sulaiman, Experimental study of melting and solidification of PCM in a triplex tube heat exchanger with fins, Energy Build. 68 (2014) 33–41.

[25] A.R. Darzi, M. Farhadi, K. Sedighi, Numerical study of melting inside concentric and eccentric horizontal annuli, Appl. Math. Model. 36 (2012) 4080–4086.

[26] A.D. Brent, V.R. Voller, K.J. Reid, Enthalpy-porosity technique for melting convection diffusion phase change: application to the melting of a pure metal, Numer. Heat Transfer 13 (1988) 297–318.

[27] C. Guo, W. Zhang, Numerical simulation and parametric study on a new type of high-temperature latent heat thermal energy storage system, Energy Convers. Manage. 49 (2008) 919–927.

[28] M. Hosseini, A. Ranjbar, K. Sedighi, M. Rahimi, A combined experimental and computational study on the melting behavior of a medium-temperature phase change storage material inside a shell-and-tube heat exchanger, Int. Commun. Heat Mass Transfer 39 (2012) 1416–1424.

[29] W.-B. Ye, D.-S. Zhu, N. Wang, Numerical simulation on phase-change thermal storage/release in a plate-fin unit, Appl. Thermal Eng. 31 (2011) 3871–3884.

[30] S.V. Patankar, Numerical Heat Transfer and Fluid Flow, McGraw Hill, New York, 1980.

[31] A.A. Al-Abidi, S.B. Mat, K. Sopian, M.Y. Sulaiman, A.T. Mohammad, CFD applications for latent heat thermal energy storage: a review, Renew. Sust. Energy Rev. 20 (2013) 353–363.

[32] S.F. Hosseinizadeh, A.A.R. Darzi, F.L. Tan, Numerical investigations of unconstrained melting of nano-enhanced phase change material (NEPCM) inside a spherical container, Int. J. Therm. Sci. 51 (2012) 77–83.